Stochastic dynamics of a Brownian motor based on morphological changes

F. Ambía and H. Híjar
Grupo de Sistemas Inteligentes, Facultad de Ingeniería,
Universidad La Salle, Benjamín Franklin 47, 06140, Ciudad de México.

Received 16 February 2017; accepted 18 April 2017

We introduce a simplified model for a microscopic system that performs directed Brownian motion due to coordinated morphological adaptations. This system consists of two spherical particles with adaptable size, that interact through elastic and repulsive forces. We propose an algorithm to control the time dependence of the system's shape that turns it into a Brownian motor, whose stochastic dynamics is analyzed by means of a Langevin model. We restrict ourselves to the simplified case of motors with small shape asymmetries and slow morphological changes, and calculate the average speed at which they should move. We compare the theoretical predictions with the results from Brownian Dynamics simulations and find that they are in very good quantitative agreement. We carry out a comparison of the proposed rectifying algorithm with a classical one based on a ratchet potential and show that in some cases morphological adaptations could produce larger velocities. We thus propose the locomotion mechanism based on controlled structural changes as a novel alternative method from which Brownian motors could operate autonomously, *i.e.*, requiring neither a substrate nor a ratchet field.

Keywords: Brownian motor; Langevin dynamics; rectified Brownian motion.

PACS: 05.40.Jc; 05.40.-a; 05.70.Ln

1. Introduction

In accordance with the second law of thermodynamics, it is not possible to obtain a net current of Brownian particles when they are subjected only to equilibrium thermal forces [1–3]. However, in the presence of ratchets or intelligent control systems, *e.g.*, a Maxwell's demon, Brownian motion can be rectified and a current of Brownian particles can be generated which is maintained by the unbiased fluctuating forces exerted by the thermal bath [4]. Understanding the precise mechanisms that allow a microscopic system to perform directed Brownian motion in an isotropic noisy environment, is a problem that has received considerable attention during the last decades [5–7]. The interest on this subject has increased since the discovery that life processes are conducted by Brownian motors or *molecular machines*, that perform multiple specialized tasks in the cells of living organisms [8]. Examples of such molecular motors include: kinesins [9, 10], ATP synthases [11–13], and helicases [14, 15]. It is now known that these machines are sophisticated molecular structures that use the spontaneous fluctuations occurring in their surroundings together with ratchet mechanisms, in order to break the spatial symmetry of their dynamics [16].

From the theoretical point of view, many models have been formulated through the years that predict the emergence of directed Brownian motion from unbiased noise, most of which are based on the use of a *ratchet potential*, *i.e.*, a periodic potential that lacks reflection symmetry. Even in absence of spatial symmetry, a net drift of a Brownian particle is forbidden by the second law. However, if the particle is in the presence of an additional force having time correlations, detailed balance is broken and a non-vanishing drift is produced [3]. A resembling situation occurs when a Brownian particle in a ratchet potential is immersed in a bath with a temperature that changes in time periodically [17]. In this case, detailed balance is lost as a consequence of temperature variations and directed motion is achieved having no other source than thermal fluctuations [18]. In a very similar fashion, Brownian motion can be rectified by producing cyclic variations of the amplitude of the substrate potential [6]. The so-called Stokes' drift, a deterministic mechanism that drags along particles suspended in a viscous medium traversed by a longitudinal wave [19], can be also used together with time-dependent unbiased forces to achieve the Brownian motor behavior [20]. In addition to these examples, a great variety of non-equilibrium perturbations exist that can be used for propelling a Brownian motor, in which a ratchet potential is not involved. This is the case discussed in the excellent review in Ref. 7, of using stochastic non-equilibrium perturbations with vanishing mean but higher order odd moments different from zero.

Thanks to the theoretical analysis of these mechanisms, it has been possible to formulate a general definition of a Brownian motor based on the role that the breakdown of symmetries and fluctuations play in its operation [6, 7]. According to this definition, a genuine Brownian motor is any physical system supplemented with a rectification mechanism that is critically affected by the spatio-temporal periodicity, on which all the forces and gradients average zero, and which is kept away from thermodynamic equilibrium by the rupture of the detailed balance symmetry. Most importantly, in order to constitute an authentic Brownian motor, the random forces acting on the system, having thermal or non-thermal origin, must assume a principal role.

Models of directed Brownian motion could lead in the future to the fabrication of micro and nanomachines aimed at functions such as: targeted drug delivery [21,22]; stirring and pumping in microfluidic devices and biological systems [22]; and separation of colloids, macromolecules, chromosomes or

viruses [23–25]. Although, up to now, diverse artificial autonomous micromotors have been realized, some of which are powered by catalytic reactions [26], Janus particles [27], or micro-electromechanical technologies [28], the operation of these nanoscale devices is controlled mainly by deterministic mechanical or chemical forces, and thermal noise does not necessarily play a major role [7]. The case is the same for some theoretical models of microsystems that perform efficient locomotion in viscous fluids [29–31]. What is worse, thermal fluctuations are even considered as problematic when such microdevices are designed, since molecular collisions might alter their desired trajectories [22]. We will show here that, in contrast to this point of view, thermal forces could be used as a source to propel a theoretical elastic motor that advances by adapting its shape according to the configuration that the same thermal forces produce.

Specifically, in this paper we will analyze in detail the fluctuating dynamics of a theoretical Brownian motor that, as far as we can tell, has only been studied by ourselves in terms of a very basic formulation [32]. This model consists of an elastic system with adaptable shape that can be propelled by thermal noise and coordinated unbiased morphological changes, without needing for a ratchet potential. We will study the statistical properties of the system in terms of a Langevin model in Sec. 2 restricting ourselves to the case of motors with purely elastic interactions and having small and slow morphological modifications. From this model we will be able to obtain an explicit expression for the average speed of the motor. In Sec. 3 we will implement Brownian Dynamics simulations that corroborate the theoretical predictions within the limit corresponding to the approximations of the model. Afterwards in Sec. 4, we will extend our model and simulation procedure to supplement them with features that are commonly found in microscopic systems, namely: intermolecular repulsive interactions and finite nonlinear elastic forces. This has the purpose of showing that it is plausible to think on an actual physical realization of our proposal. For this extended case, we will be able to give again an expression for the average motor's velocity, which is found to be in very good quantitative agreement with the results of the numerical implementation. Finally, in Sec. 6 we will summarize our main conclusions.

2. Directed Brownian motion from morphological adaptations

2.1. Basic algorithm for directed motion

We will review first the basic idea for the operation of our Brownian motor based on morphological changes, as it was introduced in Ref. 32. The model is constituted by two spherical particles, with identical mass m, that perform one-dimensional Brownian motion along the x direction, in a fluid with viscosity η and temperature T. The symbols x_1 and R_1 denote, respectively, the position of the center and the radius of the first sphere, while x_2 and R_2 indicate the corresponding quantities of the second one. The particles interact through the elastic potential, $U = k\left(x_2 - x_1 - l\right)^2/2$, where k is the restitution coefficient and l is an equilibrium distance, representing the average elongation of the complete system. As it is usual, the dynamics of the system is described using the low Reynolds number approximation, since viscous forces are expected to be much larger than inertial contributions. Under such conditions, the mass is not relevant on the dynamics of the particles and their stochastic equations of motion can be cast in the form

$$\frac{dx_{\text{c.m.}}}{dt} = -\frac{k}{2}\left(\frac{1}{\beta_2} - \frac{1}{\beta_1}\right)\left(x_{\text{r}} - l\right) + \frac{1}{2}\left(\frac{1}{\beta_1}A_1 + \frac{1}{\beta_2}A_2\right), \quad (1)$$

$$\frac{dx_{\text{r}}}{dt} = -k\left(\frac{1}{\beta_1} + \frac{1}{\beta_2}\right)\left(x_{\text{r}} - l\right) + \frac{1}{\beta_2}A_2 - \frac{1}{\beta_1}A_1. \quad (2)$$

In the first place, notice that the previous equations have been written in terms of the the center of mass position, $x_{\text{c.m.}} = \left(x_1 + x_2\right)/2$, and the current extension of the motor, $x_{\text{r}} = x_2 - x_1$. In addition, $\beta_\mu = 6\pi\eta R_\mu$, (throughout this paper Greek indices will run over the values 1 and 2), represent the drag coefficients on the spheres assuming no-slip boundary conditions at their surfaces. Moreover, in Eqs. (1) and (2), A_μ, denotes the stochastic force acting on the μth particle, which satisfies $\langle A_\mu \rangle = 0$, and the usual fluctuation-dissipation relation

$$\langle A_\mu\left(t'\right) A_\nu\left(t\right)\rangle = 2k_B T\beta_\mu \delta\left(t' - t\right)\delta_{\mu\nu}. \quad (3)$$

where k_B is the Boltzmann constant; and no summation over repeated indices is implied.

In the model described in Ref. 32, it is assumed that the configuration of the motor is maintained constant over an entire interval of time, say from time 0 to time t. In this interval, the formal solution of Eqs. (1) and (2) is given by

$$\begin{aligned} x_{\text{c.m.}} = {} & x^o_{\text{c.m.}} + \tilde{\eta}\left(1 - e^{-\alpha t}\right)\left(x^o_{\text{r}} - l\right) \\ & + \int_0^t d\xi \Big[\psi^{(1)}_{\text{c.m.}}\left(t - \xi\right) A_1\left(\xi\right) \\ & + \psi^{(2)}_{\text{c.m.}}\left(t - \xi\right) A_2\left(\xi\right)\Big], \end{aligned} \quad (4)$$

$$\begin{aligned} x_{\text{r}} = {} & l + \left(x^o_{\text{r}} - l\right) e^{-\alpha t} + \int_0^t d\xi \left[\psi^{(1)}_{\text{r}}\left(t - \xi\right) A_1\left(\xi\right)\right. \\ & \left. + \psi^{(2)}_{\text{r}}\left(t - \xi\right) A_2\left(\xi\right)\right], \end{aligned} \quad (5)$$

where $x^o_{\text{c.m.}}$ and x^o_{r} are the initial values of $x_{\text{c.m.}}$ and x_{r}, respectively; $\alpha = k\left(\beta_1^{-1} + \beta_2^{-1}\right)$, and $\tilde{\eta} = \left(R_2 - R_1\right)/2\left(R_1 + R_2\right)$; and the auxiliary functions $\psi^{(\mu)}_{\text{c.m.}}$, $\psi^{(\mu)}_{\text{r}}$, are given by

$$\psi_{\text{c.m.}}^{(\mu)}(t) = \left[\frac{e^{-\alpha t}}{2\beta_\mu} + \frac{1-e^{-\alpha t}}{\beta_1+\beta_2}\right],$$

$$\text{and} \quad \psi_{\text{r}}^{(\mu)}(t) = (-1)^\mu \frac{e^{-\alpha t}}{\beta_\mu}. \tag{6}$$

Observe from Eq. (4) that an average displacement of $x_{\text{c.m.}}$ will occur whenever $\tilde{\eta} \neq 0$ and $x_{\text{r}}^o \neq l$. That is, when the particles have different sizes, the bigger one experiences a larger viscous drag and plays the role of anchor for the motor, while the smaller one is able to move and, by the effect of the elastic interaction, produces the displacement of $x_{\text{c.m.}}$. Such displacement will tend to occur in the direction dictated by the sign of $\tilde{\eta}(x_{\text{r}} - l)$. This result suggests that thermal forces and morphological changes can be combined in favor of producing directed motion. The main idea is to use the fact that stochastic forces will drive x_{r} away from l persistently, and to supplement the motor with an intelligent control system that breaks detailed balance by measuring x_{r} and producing a variation of R_1 and R_2 in such a way that the product $\tilde{\eta}(x_{\text{r}} - l)$ will have a preferred sign during the whole evolution of the system.

In Ref. 32, it was assumed that R_1 and R_2 can be switched between two prescribed values R_{max}, and R_{min} ($R_{\text{max}} > R_{\text{min}}$), according to the rule

$$\begin{array}{llllll} R_1 = R_{\text{max}}, & \text{and} & R_2 = R_{\text{min}}, & \text{if} & x_{\text{r}} < l; \\ R_1 = R_{\text{min}}, & \text{and} & R_2 = R_{\text{max}}, & \text{if} & x_{\text{r}} > l. \end{array} \tag{7}$$

which guarantees that the tendency of $x_{\text{c.m.}}$ will be to move along the positive direction, as it is illustrated in Fig. 1.

One of the main results in Ref. 1 is that the basic rectification algorithm described by Eq. (1) makes the motor able to move at a constant average speed. Such speed increases

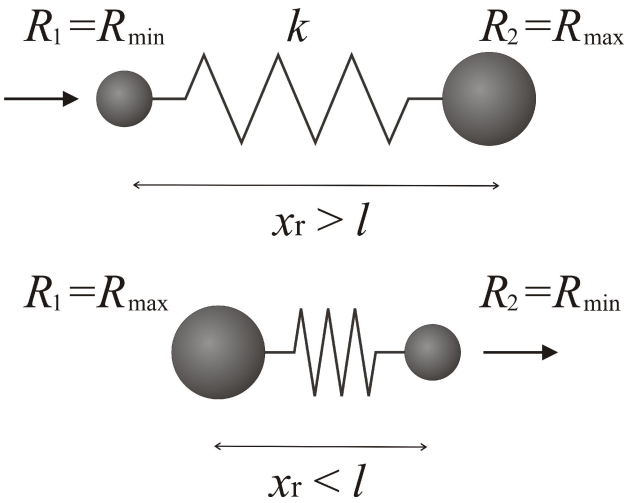

FIGURE 1. Basic algorithm for a Brownian motor based on morphological changes. The sphere with radius R_{max} acts as anchor, while the one with radius R_{min} moves as a consequence of the elastic interaction represented by the spring. Thermal forces produce the changes in the elongation of the system and coordinated shape adaptations produce the center of mass displacement in the direction indicated by the broader arrows.

with the temperature, the difference $\Delta R \equiv R_{\text{max}} - R_{\text{min}}$, and the elastic coefficient of the motor, while it decreases with the viscosity of the surrounding medium, see Eq. (9) in Ref. 32. In addition it is found that the standard deviation of the distribution function for the position of an ensemble of motors increases linearly with time.

2.2. Morphological changes at finite times and hydrodynamic effects

The model discussed so far, is not completely satisfactory from the physical point of view for two principal reasons. First, it requires for instantaneous changes in the shape of the motor. Second, it does not take into account the flow produced around the spheres as a consequence of these changes. In favor of analyzing a more consistent situation, we will assume now that the update of the radii R_μ between the values R_{min} and R_{max}, occurs at finite time intervals of characteristic duration τ_{R}. An appealing way to model such changes is to assume that, when the condition for a modification in shape is met, R_1 and R_2 go from their current values to R_{min} or R_{max} exponentially. Accordingly, we propose to update the sizes of the spheres 1 and 2 as follows:

$$\begin{aligned} &\text{if} \quad x_{\text{r}} > l \quad \text{then} \\ &R_1(t) = R_1(t_p)\, e^{-\zeta(t-t_p)} + R_{\text{min}}\left(1 - e^{-\zeta(t-t_p)}\right), \\ &R_2(t) = R_2(t_p)\, e^{-\zeta(t-t_p)} + R_{\text{max}}\left(1 - e^{-\zeta(t-t_p)}\right); \\ &\text{if} \quad x_{\text{r}} < l \quad \text{then} \\ &R_1(t) = R_1(t_p)\, e^{-\zeta(t-t_p)} + R_{\text{max}}\left(1 - e^{-\zeta(t-t_p)}\right), \\ &R_2(t) = R_2(t_p)\, e^{-\zeta(t-t_p)} + R_{\text{min}}\left(1 - e^{-\zeta(t-t_p)}\right); \end{aligned} \tag{8}$$

in which $\zeta = \tau_{\text{R}}^{-1}$, t_p denotes the instant at which the pth structural change takes place, and $t_p \leq t \leq t_{p+1}$.

On the other hand, hydrodynamic effects can be incorporated in a similar way as it is done in the case of microswimmer models [30, 31]. More precisely, if we limit ourselves to study very elongated motors with geometric features satisfying the inequality $R_\mu/l \ll 1$, then the flow around the system of two spheres can be obtained, by the linearity of the Stokes equations, as the superposition of the flow around the individual spheres [31]. By noticing that the flow produced by an expanding sphere increases with the time derivative of its volume and decreases with the square of the distance from its center [33], we find, under the previous assumption, that $x_{\text{c.m.}}$ and x_{r} obey the following system of coupled Langevin equations

$$\begin{aligned} \frac{dx_{\text{c.m.}}}{dt} = &-\frac{k}{2}\left(\frac{1}{\beta_2} - \frac{1}{\beta_1}\right)(x_{\text{r}} - l) + \frac{1}{8\pi x_{\text{r}}^2}\left(\dot{V}_1 - \dot{V}_2\right) \\ &+ \frac{1}{2}\left(\frac{1}{\beta_1}A_1 + \frac{1}{\beta_2}A_2\right), \end{aligned} \tag{9}$$

$$\frac{dx_{\rm r}}{dt} = -k\left(\frac{1}{\beta_1}+\frac{1}{\beta_2}\right)(x_{\rm r}-l) + \frac{1}{4\pi x_{\rm r}^2}\left(\dot{V}_1+\dot{V}_2\right)+\frac{1}{\beta_2}A_2-\frac{1}{\beta_1}A_1. \quad (10)$$

Here, $\dot{V}_1$ and $\dot{V}_2$ represent the rates of change of the volumes of spheres 1 and 2, respectively. The terms containing these quantities in Eqs. (9) and (10) represent the influence that the expanding and contracting spheres have on each other through the fluid that surrounds them. When those terms are neglected, Eqs. (9) and (10) reduce to Eqs. (1) and (2). Moreover, if morphological changes were such that the total volume of the motor is conserved, then $\dot{V}_1 = -\dot{V}_2$, and Eq. (9) would take a form resembling Eq. (1.1) in Ref. 31, but supplemented with the contribution of the stochastic forces on the spheres. Another important attribute of Eqs. (9) and (10) is that they are non-linear, in contrast with Eqs. (1) and (2), as a consequence of the hydrodynamic interaction. Furthermore, notice that in Eqs. (9) and (10) β_μ and $\dot{V}_\mu$, depend on time implicitly through their dependence on $R_\mu(t)$.

It is worth stressing that during the operation of efficient Brownian motors, detailed balance symmetry, which governs the dynamics around equilibrium, must be broken by forcing these motors to operate away from thermal equilibrium [7]. In the case of our motor based on morphological changes, departure from equilibrium is promoted by the adaptations in shape themselves. Put differently, if such adaptations were not performed, the coefficients β_1 and β_2 in Eqs. (9) and (10) would take constant values, while $\dot{V}_1$ and $\dot{V}_2$ would vanish. In that case, $x_{\rm r}$ and $x_{\rm c.m.}$ would relax from their initial values towards thermodynamic equilibrium where all dynamics would be governed by detailed balance. There, as it can be inferred from Eqs. (4) and (5), no net average displacement of $x_{\rm c.m.}$ would occur. In contrast, morphological changes take the motor away from equilibrium persistently thus braking detailed balance. They also provide the combination of asymmetry and non-equilibrium forces, necessary for the production of constructive transport.

The appearance of the stochastic forces in Eqs. (9) and (10) deserves a special comment, since when R_1 and R_2 are time-dependent, the system is not in equilibrium and the usual fluctuation-dissipation theorem, Eq. (3), is not suitable. We will assume, that R_1 and R_2 exhibit significant variations over a time-scale that is large compared with the time-scale of thermal noise. Accordingly, it could be expected that the fluctuation-dissipation relation will be valid instantaneously, and we propose to write it in the form

$$\left\langle \frac{A_\mu(t')}{\beta_\mu(t')}\frac{A_\nu(t)}{\beta_\nu(t)}\right\rangle = \frac{2k_BT}{\beta_\mu(t)}\delta(t'-t)\,\delta_{\mu\nu}. \quad (11)$$

In this paper we will restrict ourselves to analyze the dynamics resulting from Eqs. (9) and (10) in the limiting case of small morphological changes, determined by the condition $\Delta R/R_{\rm min} \equiv \Delta \ll 1$. Apart from being very convenient from the mathematical point of view, this case could be interesting since it will exhibit that our motor is able to perform directed Brownian motion even when it does not have a strong geometrical asymmetry.

In addition, when configuration changes occur at finite times, R_1 and R_2 will spend time far from their limiting values $R_{\rm min}$ and $R_{\rm max}$. The departure of R_1 and R_2 from $R_{\rm min}$ and $R_{\rm max}$, will depend on $\tau_{\rm R}$, as well as on the characteristic time for which the conditions in Eq. (8) subsist, $\bar{\tau}$. Notice that, physically, $\bar{\tau}$ is determined by the strength of the elastic interaction and the viscosity of the fluid, while $\tau_{\rm R}$ is a parameter that depends on the motor's structure and that, consequently, can be theorized. In the present paper, we will analyze the case of motors that adapt their morphology slowly, in such a way that $\bar{\tau} \ll \tau_{\rm R}$. Thus, the time-scale for morphological adaptations can be considered as a fast scale, and Eqs. (9) and (10) can be simplified by averaging over these fast processes. In this situation and assuming that the system starts in a condition such that $x_{\rm r} > l$, we have

$$R_2(t)-R_1(t) \simeq \int_0^\infty d\tau\, P(\tau)\,[R_2(\tau)-R_1(\tau)] \simeq (-1)^p\,\Delta R\,(1-2\zeta\bar{\tau}), \quad (12)$$

and

$$\dot{V}_2(t)-\dot{V}_1(t) \simeq \int_0^\infty d\tau\, P(\tau)\left[\dot{V}_2(\tau)-\dot{V}_1(\tau)\right] \simeq (-1)^p\,8\pi\zeta\Delta R\,R_{\rm min}^2, \quad (13)$$

where $P(\tau)$ is the probability distribution function (PDF) for observing that the conditions in Eq. (8) last a time interval τ, to be specified at the end of this section. In order to obtain the previous results, we have used the explicit form of R_1 and R_2, given by Eq. (8), neglected quadratic and higher order contributions in ΔR and $\zeta\bar{\tau}$, and assumed that R_1 and R_2 remain close to their limiting values $R_{\rm min}$ and $R_{\rm max}$.

Another simplifying assumption will consist in considering that the thermal fluctuations in $x_{\rm r}$ are small as compared with the total elongation of the system. In other words, if $\tilde{x}_{\rm r}(t) \equiv x_{\rm r}(t) - l$, represents the spontaneous change in the length of the motor, then we will suppose that $\tilde{x}_{\rm r}/l \ll 1$.

By expanding Eqs. (9) and (10) up to the first order in the previously defined small quantities, it can be verified that in the interval $t_p \le t \le t_{p+1}$, they reduce to

$$\frac{dx_{\rm c.m.}}{dt} = (-1)^p\tilde{\eta}_1\Delta R\,(1-2\zeta\bar{\tau})\,\tilde{x}_{\rm r} - (-1)^p\varepsilon^2\zeta\Delta R + \frac{1}{2}\left(\frac{A_1}{\beta_1}+\frac{A_2}{\beta_2}\right), \quad (14)$$

and

$$\frac{d\tilde{x}_{\rm r}}{dt} = -\alpha_1\tilde{x}_{\rm r}+\frac{A_2}{\beta_2}-\frac{A_1}{\beta_1}, \quad (15)$$

respectively, where we have introduced the definitions $\tilde{\eta}_1 = k/12\pi\eta R_{\rm min}^2$, $\varepsilon = R_{\rm min}/l$, and $\alpha_1 = k(2-\Delta)/6\pi\eta R_{\rm min}$.

First, we notice that within the range of applicability of the performed approximations, $\tilde{x}_{\rm r}$ follows the usual stochastic process for a harmonically bound Brownian particle in an equilibrium environment in the overdamped regime [34]. Therefore, the PDF for observing $\tilde{x}_{\rm r}(t')$ at time t', given that it was found to be $\tilde{x}_{\rm r}(t)$ at time t is

$$W\left(\tilde{x}_{\rm r}(t')\,|\tilde{x}_{\rm r}(t)\right)=\frac{1}{\sqrt{2\pi\sigma_{\rm r}^2(t'-t)}}\times\exp\left\{-\frac{\left[\tilde{x}_{\rm r}(t')-l-e^{-\alpha_1(t'-t)}\tilde{x}_{\rm r}(t)\right]^2}{2\sigma_{\rm r}^2(t'-t)}\right\},\quad(16)$$

with $\sigma_{\rm r}^2(t'-t)=k_BT\left(1-e^{-2\alpha_1(t'-t)}\right)/k$. In the asymptotic limit, this distribution reduces to the stationary distribution

$$W(x_{\rm r})=\sqrt{\frac{k}{2\pi k_BT}}\exp\left\{-\frac{k\,(x_{\rm r}-l)^2}{2k_BT}\right\}.\quad(17)$$

Notice that the fluctuations of $\tilde{x}_{\rm r}$ according to this distribution are responsible for promoting the advance of the motor when they are coupled with morphological changes though Eq. (14). For the sake of quantifying this effect, we will consider the evolution of $x_{\rm c.m.}$ over a long period of time.

It should be remarked, that under such circumstances, the hydrodynamic forces do not produce a net displacement of $x_{\rm c.m.}$, because they are symmetric and act along opposite directions for the two possible configurations of the motor (elongated or contracted). More precisely, hydrodynamic forces always point in the direction of the contracting sphere [31]. Now in this simplyfied version of Eq. (14), over a long evolution time, equal number of symmetric contractions and expansions contribute with hydrodynamic forces and the average of these forces will vanish. This will not be the case in the extended model for a molecular Brownian motor to be considered in Sec. 4. By the moment, in favor of simplifying the subsequent analysis, the term in Eq. (14) containing the factor ε^2 will be neglected. In this case, the formal solution of Eq. (14) is, up to first order in the small quantity Δ,

$$\begin{aligned}x_{\rm c.m.}(t')=x_{\rm c.m.}(t)&+(-1)^p(1-2\zeta\bar{\tau})\left(1+\frac{\Delta R}{2R_{\rm min}}\right)\\&\times\frac{\Delta}{4}\left(1-e^{-\alpha_1(t'-t)}\right)|x_{\rm r}(t)-l|\\&+\int_t^{t'}d\xi\left[\Psi_1(t'-\xi;\alpha_1)\frac{\mathcal{A}_1(\xi)}{\beta_1(\xi)}\right.\\&\left.+\Psi_2(t'-\xi;\alpha_1)\frac{\mathcal{A}_2(\xi)}{\beta_2(\xi)}\right],\end{aligned}\quad(18)$$

where

$$\Psi_1(t;\alpha_1)=\frac{1}{2}-(-1)^p(1-2\zeta\bar{\tau})\frac{\Delta}{4}(1-e^{-\alpha_1 t}),\quad(19)$$

and

$$\Psi_2(t;\alpha_1)=\frac{1}{2}+(-1)^p(1-2\zeta\bar{\tau})\frac{\Delta}{4}\left(1-e^{-\alpha_1 t}\right).\quad(20)$$

From Eqs. (18)-(20) we find the PDF for observing $x_{\rm c.m.}(t')$ at time t', given the initial conditions $x_{\rm c.m.}(t')$ and $x_{\rm r}(t)$, which is

$$W\left(x_{\rm c.m.}(t')\,|x_{\rm c.m.}(t)\,;x_{\rm r}(t)\right)=\frac{1}{\sqrt{2\pi\sigma^2}}\times\exp\left\{-\frac{\left[x_{\rm c.m.}(t')-x_{\rm c.m.}(t)-h\,|x_{\rm r}-l|\right]^2}{2\sigma^2}\right\},\quad(21)$$

where h is a function of $\bar{\tau}$ and $t'-t$, defined as $h=h(\bar{\tau};t'-t)=(1-2\zeta\bar{\tau})(1-e^{-\alpha(t'-t)})\Delta/4$.

In order to give an approximated description of the stochastic process followed by $x_{\rm c.m.}$ over a long time interval, $[0,t]$, we subdivide it into N smaller regular intervals of size $\bar{\tau}=t/N$, and identify the intermediate times as $t_q=q\bar{\tau}$, with $q=0,1,\ldots,N$. We assume that we perform N observations of the state of the system at times $t_0,t_1,\ldots,t_{N-1}$, at which $|x_{\rm r}-l|$ takes values sampled from its equilibrium distribution, Eq. (17). Then, we calculate the conditional probability for observing the motor at position $x_{\rm c.m.}(t_{q+1})$ before the beginning of the next interval, given the initial center of mass position at time t_q,

$$W\left(x_{\rm c.m.}(t_{q+1})\,|x_{\rm c.m.}(t_q)\right)=\int dx_{\rm r}\times W\left(x_{\rm c.m.}(t_{q+1})\,|x_{\rm c.m.}(t_q)\,;x_{\rm r}(t_q)\right)W\left(x_{\rm r}(t_q)\right).\quad(22)$$

By using Eqs. (17), and (18)-(22) we find that in the limit $\Delta\ll 1$, this probability can be approximated by a Gaussian that explicitly reads as

$$W\left(x_{\rm c.m.}(t_{q+1})\,|x_{\rm c.m.}(t_q)\right)=\frac{1}{\sqrt{2\pi\sigma^2_{\rm c.m.}(\bar{\tau})}}\times\exp\left\{-\frac{\left[x_{\rm c.m.}(t_{q+1})-x_{\rm c.m.}(t_q)-\chi(\bar{\tau})\right]^2}{2\sigma^2_{\rm c.m.}(\bar{\tau})}\right\},\quad(23)$$

where

$$\sigma^2_{\rm c.m.}(\bar{\tau})=\frac{k_BT}{6\pi\eta R_{\rm min}}\left(1-\frac{\Delta}{2}\right)\bar{\tau},\quad(24)$$

and

$$\chi(\bar{\tau})=\sqrt{\frac{2}{\pi}}\frac{k_BT}{k}h(\bar{\tau},\bar{\tau}).\quad(25)$$

Finally, we assume that process described by $x_{\rm c.m.}$ is of the Markov type and using the Chapman-Kolmogorov equation,

$$W\left(x_{\rm c.m.}(t)\,|x_{\rm c.m.}(0)\right)=\int dx_{N-1}dx_{N-2}\cdots dx_1\prod_{q=0}^{N-1}\times W\left(x_{\rm c.m.}(t_{q+1})\,|x_{\rm c.m.}(t_q)\right),\quad(26)$$

we find the conditional PDF to observe the motor at a position $x_{\text{c.m.}}(t)$ at the end of the process, given that it was at $x_{\text{c.m.}}(0)$ at the beginning. Such PDF is

$$W\left(x_{\text{c.m.}}(t)\,|x_{\text{c.m.}}(0)\right) = \frac{1}{\sqrt{2\pi\sigma^2_{\text{c.m.}}(t)}} \times \exp\left\{-\frac{\left[x_{\text{c.m.}}(t) - x_{\text{c.m.}}(0) - N\chi(\bar{\tau})\right]^2}{2\sigma^2_{\text{c.m.}}(t)}\right\}, \quad (27)$$

It will be discussed in the subsequent Sec. 3 that, in general, the relaxation time α_1^{-1} takes values that are much larger than $\bar{\tau}$ and, consequently, the approximation $\alpha_1\bar{\tau} \ll 1$ is valid, from which we can write $N\chi(\bar{\tau}) = v_{\text{c.m.}}t$, that defines the average velocity of the motor

$$v_{\text{c.m.}} = \frac{1-2\zeta\bar{\tau}}{6\sqrt{2}\pi^{3/2}}\frac{\Delta R}{R^2_{\text{min}}}\frac{\sqrt{k\,k_BT}}{\eta}. \quad (28)$$

In order to finish the analysis of the present model, we will discuss how the characteristic time $\bar{\tau}$, appearing in Eqs. (27) and (28), can be estimated. It can be seen from Eq. (8), that $\bar{\tau}$ can be interpreted as the average of the time elapsed between two successive observations of the value $x_{\text{r}} = l$. Under the approximations leading to Eq. (17), $\bar{\tau}$ is also the mean time needed by a harmonically constrained Brownian particle for consecutively crossing over the potential's minimum. According to general theory for first exit times in harmonic potentials [35], the PDF for observing two consecutive values $x_{\text{r}} = l$, occurring in a time interval τ is given by

$$P(\tau) = -\frac{\partial S(\tau)}{\partial\tau}, \quad (29)$$

where $S(\tau)$ is the *survival probability*, *i.e.*, the probability for observing the confined particle at $x_{\text{r}} = l$, at time $t = 0$, and at the same position at a subsequent time $t = \tau$, under the condition that it has not passed over this point at any intermediate time. If we restrict ourselves to consider short times τ, *i.e.*, times satisfying the condition $\alpha_1\tau \ll 1$, the function $S(\tau)$ can be obtained from the transition probability $W\left(\tilde{x}_{\text{r}}(t')\,|\tilde{x}_{\text{r}}(t)\right)$, as it is given by Eq. (16). Specifically, we have

$$S(\tau) = \int_0^\infty dx'_{\text{r}} W\left(x_{\text{r}}(\tau) = l\,|x'_{\text{r}}(\tau_1)\right) W\left(x'_{\text{r}}(\tau_1)|x_{\text{r}}(0) = l\right)$$
$$= \left[2\pi\left(\sigma^2_{\text{r}}(\tau-\tau_1) + e^{-2\alpha_1(\tau-\tau_1)}\sigma^2_{\text{r}}(\tau_1)\right)\right]^{-1/2}, \quad (30)$$

where $0 \le \tau_1 \le \tau$. By expanding Eq. (30) in terms of the small quantity $\alpha_1\tau$, and retaining only the leading contribution, we find that $S(\tau) = (k/4\pi k_BT\alpha_1\tau)^{1/2}$, and consequently, $P(\tau)$ turns out to be

$$P(\tau) = \frac{1}{2}\tau_{\text{min}}^{1/2}\tau^{-3/2}, \quad (31)$$

which is a special case of the so-called Pareto distribution.

This result is valid only for $\tau > \tau_{\text{min}}$, where τ_{min} is a quantity introduced to guarantee that $P(\tau)$ is correctly normalized. Physically, it could be expected that such a minimum time for the validity of Eq. (31) must exist, since the analysis that conducted to this result is valid only in a timescale that is larger than the one corresponding to the rapidly fluctuating force of the solvent [36].

It is well known that for the power law distribution function given by Eq. (31), it is not possible to find an analytical expression for its mean value [37]. Therefore, we will estimate $\bar{\tau}$ following a numerical procedure based on the results of BD simulations. To be specific, we will show in the subsequent section 3. that the PDF for τ can be very well adjusted by Eq. (31), and use the time series of values of x_{r} to determine both, τ_{min} and $\bar{\tau}$.

3. Brownian Dynamics Simulations

With the purpose of analyzing the validity of the model described in Sec. 2, we implemented a BD simulation scheme that allowed us to solve Eqs. (9) and (10) numerically. Our implementation consisted of a temporal discretization method in which we fixed $R_{\text{min}} = 1$, $m = 1$, and $k_BT = 1$, as the units of length, mass, and energy, respectively. Notice that under such conditions, units of time, u_{t}, are not independent but given by $u_{\text{t}} = R_{\text{min}}\sqrt{m/k_BT}$. The numerical integration of Eqs. (9) and (10) was carried out using a time-step with size $\Delta t = 10^{-3}u_{\text{t}}$. In the numerical scheme, stochastic forces were sampled from a Gaussian distribution and actualized every two simulation steps. We performed numerical experiments varying R_{max} from $R_{\text{max}} = 1.0\,R_{\text{min}}$, to $1.25\,R_{\text{min}}$, with the purpose of showing that the coupled Brownian system depicted in Fig. 1 acquires directed motion even for small configuration changes. On the other hand, the values of the restitution coefficient and the viscosity were fixed at $k = 5\,k_BT/R^2_{\text{min}}$, and $\eta = 5\sqrt{mK_BT}/R^2_{\text{min}}$, respectively. Notice that this selection of parameters gives characteristic relaxation times $\alpha_1^{-1} \sim 10u_{\text{t}} \gg \Delta t$, which guarantee that the usual separation of time-scales of Brownian motion is properly approximated. In addition, the characteristic time for radii adaptations was chosen to be $\tau_R = 2u_{\text{t}} \gg \Delta t$.

Let us show first, that directed Brownian motion indeed appears in motors simulated under such conditions. This is done in Fig. 2, in which we present six trajectories for Brownian motors with morphological adaptations with different magnitude, reported in terms of the dimensionless parameter Δ. The noisy curves in Fig. 2 represent the numerical results. They prove that morphological changes in fact induce directed motion.

On the other hand, the straight lines in Fig. 2 were drawn using the average velocity, $v_{\text{c.m.}}$, calculated from Eq. (28). It is worth noticing that in order to obtain an estimate of $v_{\text{c.m.}}$, it is necessary to provide the average time for configurational changes, $\bar{\tau}$. As it was explained at the end of Sec. 2, $\bar{\tau}$ was calculated using the numerical results. More precisely, during the simulations that yielded the results depicted in Fig. 2,

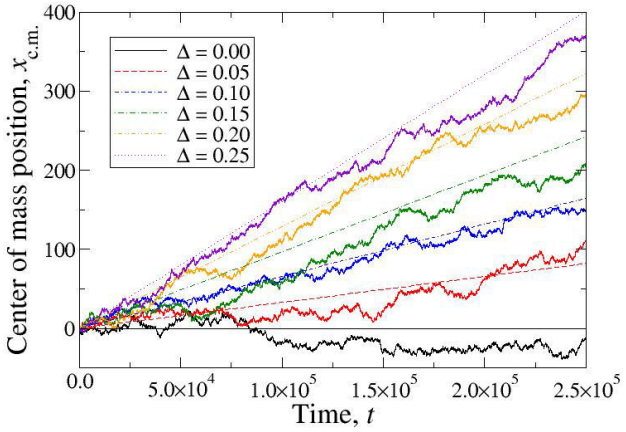

FIGURE 2. Directed Brownian motion experienced by simulated motors with different asymmetry degrees represented by the parameter Δ. Straight lines correspond with the theoretical velocity calculated from Eq. (28), while noise curves are the actual trajectories of the motors.

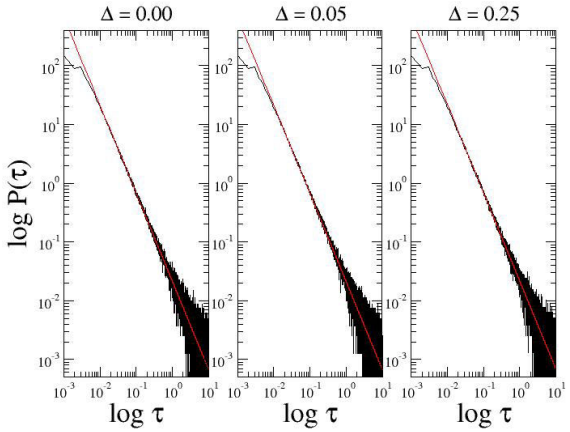

FIGURE 3. Probability distribution function for the duration of morphological configurations, $P(\tau)$. Noisy black curves represent the results of numerical experiments for the indicated values of Δ, while the red straight lines are fits obtained from the power law $P(\tau) \propto \tau^{-3/2}$. The numerical distributions are used to estimate $\bar{\tau}$.

we stored the values of the time intervals of elongated or contracted configuration, τ, from which we calculated numerically the PDF $P(\tau)$. For the experiments conducted over the time interval shown in Fig. 2, the available data for calculating $P(\tau)$ ranged from $818,342$ for $\Delta = 0.00$, to $776,089$ for the case $\Delta = 0.25$. We found that $P(\tau)$ actually follows the power law behavior predicted in Eq. (31). This fact is illustrated in Fig. 3 in which we present the numerical evaluation of $P(\tau)$ obtained for the simulation cases $\Delta = 0.00$, 0.05 and 0.25 (black noisy curves).

The straight lines shown in Fig. 3 correspond to a nonlinear fitting of the numerical data in which Eq. (31) was used by considering τ_{min} as an adjustable parameter. The specific values of τ_{min} were found to be independent on Δ, within the range of the numerical uncertainties, *e.g.*, they were $(1.85 \pm 0.03) \times 10^{-3}$, $(1.84 \pm 0.03) \times 10^{-3}$, and $(1.86 \pm 0.03) \times 10^{-3}\, u_{\text{t}}$, respectively, for the three cases illustrated in Fig. 3. On the other hand, we summarize in Table I the set of numerical values of $\bar{\tau}$ obtained from the numerical distributions $P(\tau)$, where it can be appreciated that, for the selected range of simulation parameters, $\bar{\tau}$ increases with Δ but exhibits small percental variations lower than 5%. The values of $\bar{\tau}$ shown in table I were used to calculate $v_{\text{c.m.}}$ from Eq. (28). The resulting values are shown in the third column of Table I. These were used to plot the straight lines appearing in Fig. 2.

Finally, we will show that the stochastic process describing the spatial advance of an set of simulated motors exhibits the properties predicted in Sec. 2. With this purpose, we conducted additional simulations for two ensembles of 10^4 independent motors with characteristic size asymmetries $\Delta = 0.05$, and $\Delta = 0.25$. For such ensembles, we calculated, at different simulation times, the PDF for the center of mass position, $W(x_{\text{c.m.}}(t) \mid x_{\text{c.m.}}(0) = 0)$, and compared the results with those expected from Eqs. (24), (27) and (28),

TABLE I. Average time $\bar{\tau}$ obtained from numerical experiments of motors with different morphological asymmetry factors Δ. The estimation of the mean center of mass velocity, $v_{\text{c.m.}}$, obtained from Eq. (28) is also presented.

Δ	$\bar{\tau}$ $(\pm 0.002 u_{\text{t}})$	$v_{\text{c.m.}}$ $(10^{-4}\, u_{\text{t}}/R_{\text{min}})$
0.00	0.306	0.0
0.05	0.305	3.29 ± 0.01
0.10	0.315	6.58 ± 0.02
0.15	0.317	9.69 ± 0.03
0.20	0.319	12.90 ± 0.04
0.25	0.322	16.04 ± 0.05

using the estimations of $v_{\text{c.m.}}$ presented in Table I. In addition, we calculated the standard deviation $\sigma_{\text{c.m.}}$ of the distributions observed for the ensembles as function of the simulation time and compare the numerical results with the expected behavior as given by Eq. (24). Our results are summarized in Fig. 4, where a very good agreement between the numerical and experimental results can be observed.

4. Extended model for a molecular Brownian motor

In Sec. 3, we considered a numerical method that allowed us to solve the system of stochastic Eqs. (9) and (10), and to verify the predictions of the theoretical model introduced in Sec. 2. Here, we will extend our analysis to make it able to describe the Brownian dynamics of a microscopic system which is more realistic from the physical point of view. Specifically, we will consider a model consisting of two spherical colloidal particles with radii $R_1(t)$ and $R_2(t)$, attached by a molecular chain with finite extension, l_{max}. We will suppose that the elastic potential energy stored in the system when these particles are located at positions x_1 and

$x_2 > x_1$, is given by the finite extension non-linear elastic formula

$$\Phi_{\rm e}\left(x_2 - x_1\right) = -\frac{1}{2} k\, l_{\rm max}^2 \ln\left[1 + \left(\frac{x_2 - x_1}{l_{\rm max}}\right)^2\right]. \quad (32)$$

We will assume that the colloidal particles do not interact at large distances but strongly repel each other when they get in contact. Mathematically, such interaction can be represented in terms of the Weeks-Chandler-Andersen potential [38],

$$\Phi_{\rm c}\left(x_2 - x_1\right) = \begin{cases} 4\epsilon\left[\left(\frac{\sigma}{x_2 - x_1}\right)^{12n} - \left(\frac{\sigma}{x_2 - x_1}\right)^{6n} + \frac{1}{4}\right], & \text{if } x_2 - x_1 < 2^{1/6n}\sigma; \\ 0, & \text{otherwise;} \end{cases} \quad (33)$$

where ϵ denotes the interaction strength, σ is the diameter of the interaction, and n is a positive integer that determines the hardness of the colloidal particles. Notice that when $R_1\left(t\right)$ and $R_2\left(t\right)$ change in time symmetrically, as it is the case established by the exponential algorithm Eq. (8), σ can be considered to be a constant with $\sigma = R_{\rm max} + R_{\rm min}$. We considered that the radii R_1 and R_2 tend towards $R_{\rm min}$ or $R_{\rm max}$ exponentially as prescribed by Eq. (8), with a fixed characteristic time τ_R. Notice that in Eq. (8) the parameter l indicated the length at which the morphological changes of the harmonic motor were activated. For the case of a motor that operates under the internal potentials given by Eqs. (32) and (33), this parameter is absent. Therefore, we will consider that for this case a particular elongation exists, l_0, that signals the configuration of the motor at which structural adaptations are promoted.

We observed that the selection of l_0 affects the efficiency of the motor, since when it is selected to be far from the average elongation, $\langle x_{\rm r}\rangle$, a smaller number of morphological changes takes place and the velocity of the motor is reduced. Accordingly, we propose to set $l_0 \simeq \langle x_{\rm r}\rangle$.

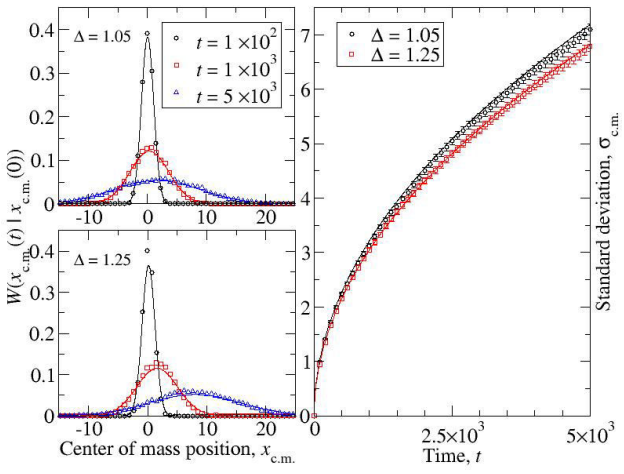

FIGURE 4. Probability distribution function for the center of mass position of an ensemble of harmonic Brownian motors at different times. Symbols correspond with the numerical results, while continuous lines were obtained from Eqs. (24), (27), and (28). The standard deviation of the distribution as function of the advance time is also shown.

An estimation of the center of mass velocity of the molecular motors defined by Eqs. (8) and (32)-(33) can be obtained by generalizing the theory presented in Sec. 2. The main differences to be taken into account with respect to our previous situation are that, in the presence of the potentials $\Phi_{\rm e}$ and $\Phi_{\rm c}$, the elongation of the system is distributed over an asymmetric probability function around $\langle x_{\rm r}\rangle$, and that the average time intervals that the motor spends in the contracted ($x_{\rm r} < \langle x_{\rm r}\rangle$) or elongated ($x_{\rm r} > \langle x_{\rm r}\rangle$) configurations will be different. These facts have two major consequences in the dynamics of the motor. First, the morphological changes, $R_2\left(t\right) - R_1\left(t\right)$, have not the same average magnitude during the time lapses for contraction and elongation. Second, the hydrodynamic forces occurring in such time intervals are no longer balanced, as it happens in the symmetric case, and they have a contribution to the center of mass velocity.

In order to quantify these effects, we will introduce a series of practical simplifications that are analogous to those leading to Eqs. (27) and (28). First, we will assume that the instantaneous morphological differences of the motor can be approximated by their average values. Using the same approximations that yielded Eqs. (12) and (13), we find in the present case

$$\left[R_2\left(t\right) - R_1\left(t\right)\right]\Big|_{\tau_\pm} \simeq \int_0^\infty d\tau P_\pm\left(\tau\right)\left[R_2\left(\tau\right) - R_1\left(\tau\right)\right] \simeq \pm\Delta R\left(1 - 2\zeta\bar{\tau}_\mp\right), \quad (34)$$

and

$$\left[\dot{V}_2\left(t\right) - \dot{V}_1\left(t\right)\right]\Big|_{\tau_\pm} \simeq \int_0^\infty d\tau P_\pm\left(\tau\right)\left[\dot{V}_2\left(\tau\right) - \dot{V}_1\left(\tau\right)\right] \simeq \pm 8\pi R_{\rm min}^2\zeta^2\Delta R\bar{\tau}_\mp, \quad (35)$$

where $P_+\left(\tau\right)$ and $P_-\left(\tau\right)$ represent, respectively, the PDF's for observing the elongated and contracted configurations extending over a period of time τ,

$$\bar{\tau}_\pm = \int d\tau\, \tau P_\pm\left(\tau\right),$$

are the corresponding mean times, and $|_{\tau_\pm}$ is used to indicate the evolution of a time-dependent function over the periods of contracted (τ_-) or elongated (τ_+) configuration.

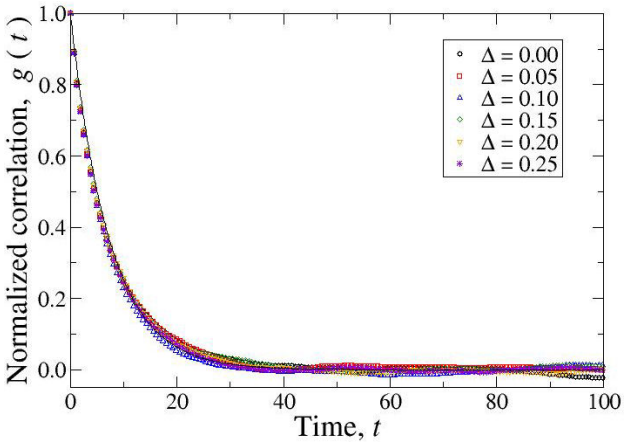

FIGURE 5. Normalized correlations for the extension of Brownian motors simulated with different asymmetry degrees, Δ, (symbols). The continuous curve represents a numerical fit obtained assuming an exponential decay.

Now, let $W_+(x_\mathrm{r})$ and $W_-(x_\mathrm{r})$ represent the partial stationary PDF's for finding x_r at $x_\mathrm{r} > \langle x_\mathrm{r}\rangle$ and $x_\mathrm{r} < \langle x_\mathrm{r}\rangle$, and $\langle x_\mathrm{r}^2\rangle_\pm$ the mean square elongation of the motor calculated over such distributions, *i.e.*,

$$\langle x_\mathrm{r}^2\rangle_\pm = \int dx_\mathrm{r}\, x_\mathrm{r}^2 W_\pm(x_\mathrm{r})\,.$$

As it was the case before, we will assume that the elongation of the system does not possess strong fluctuations. In this case, the contribution of the hydrodynamic forces to the dynamics of $x_\mathrm{c.m.}$ can be approximated by

$$-\left.\frac{\dot V_2(t)-\dot V_1(t)}{8\pi x_\mathrm{r}^2(t)}\right|_{\tau_\pm} \simeq -\frac{\left[\dot V_2-\dot V_1\right]\Big|_{\tau_\pm}}{8\pi\langle x_\mathrm{r}^2\rangle_\pm} \simeq \mp\frac{R_\mathrm{min}^2\zeta^2\Delta R\bar\tau_\mp}{\langle x_\mathrm{r}^2\rangle_\pm}\equiv\lambda_\pm. \qquad (36)$$

Another restriction to be incorporated will consist in analyzing motors with strong repulsive interactions only, which could be realized using large values of n in Eq. (33), *i.e.* $n>1$ [39]. In this case, most of the time the colloidal spheres are separated and the dynamics is dominated by the nonlinear elastic potential. It could be expected that, in this limit, x_r will evolve by following a similar relaxation behavior to the one exhibited in the simple harmonic case. However, the effective characteristic relaxation time for elongated and contracted configurations, $\alpha_\pm$, could be anticipated to be slightly different. Under such approximation and taking into account Eq. (36), an estimate for the formal solution of $x_\mathrm{c.m.}$ is

$$x_\mathrm{c.m.}(t') \simeq x_\mathrm{c.m.}(t) \pm (1-2\zeta\bar\tau_\mp)\frac{\Delta}{4}\left(1-e^{-\alpha_\pm(t'-t)}\right)\left[x_\mathrm{r}(t)-\langle x_\mathrm{r}\rangle_\pm\right]+\lambda_\pm(t'-t)$$
$$+\int_t^{t'} d\xi\left[\Psi_1(t'-\xi;\alpha_\mathrm{eff})\frac{\mathcal{A}_1(\xi)}{\beta_1(\xi)}+\Psi_2(t'-\xi;\alpha_\mathrm{eff})\frac{\mathcal{A}_2(\xi)}{\beta_2(\xi)}\right], \qquad (37)$$

where we have introduced the effective relaxation parameter, α_eff, under the assumption that α_+ and α_- are proportional to the corresponding inverse average times $\bar\tau_+$ and $\bar\tau_-$, in such a way that $\alpha_+ = \alpha_\mathrm{eff}(\bar\tau_+ + \bar\tau_-)/\bar\tau_+$, and $\alpha_- = \alpha_\mathrm{eff}(\bar\tau_+ + \bar\tau_-)/\bar\tau_-$.

If we assume, as it was done in Sec. 2.2, that we observe the dynamics of the motor over regular time intervals at which x_r is sampled from the stationary PDF's $W_\pm(x_\mathrm{r})$, that an expansion in terms of small quantities Δ and $\alpha_\pm\tau_\pm$ is valid, and that $x_\mathrm{c.m.}$ is a Markov process, we arrive at the following expression for the PDF for the advance of the motor operating over asymmetric morphological changes

$$W(x_\mathrm{c.m.}(t)\,|x_\mathrm{c.m.}(0)) = \frac{1}{\sqrt{2\pi\sigma_\mathrm{c.m.}^2(t)}} \times\exp\left\{-\frac{\left[x_\mathrm{c.m.}(t)-x_\mathrm{c.m.}(0)-v_\mathrm{c.m.}\,t\right]^2}{2\sigma_\mathrm{c.m.}^2(t)}\right\}, \qquad (38)$$

where the average center of mass velocity is given by

$$v_\mathrm{c.m.} = \alpha_\mathrm{eff}\frac{\Delta}{4}\left[(1-2\zeta\tau_-)\,\tilde x_{\mathrm{r},+}-(1-2\zeta\tau_+)\,\tilde x_{\mathrm{r},-}\right] + \frac{R_\mathrm{min}^2\zeta^2\Delta R\bar\tau_-\bar\tau_+}{\bar\tau_-+\bar\tau_+}\left(\frac{1}{\langle x_\mathrm{r}^2\rangle_+}-\frac{1}{\langle x_\mathrm{r}^2\rangle_-}\right). \qquad (39)$$

In the previous expression, we have defined the averages $\tilde x_{\mathrm{r},\pm}$ as

$$\tilde x_{\mathrm{r},\pm} = (-1)^{\mp1}\int_{\langle x_\mathrm{r}\rangle}^{\pm\infty} dx_\mathrm{r} W_\pm(x_\mathrm{r})\left[x_\mathrm{r}-\langle x_\mathrm{r}\rangle\right]. \qquad (40)$$

In Eq. (39), the first term on the right hand side is the velocity achieved by the motor due to the unbalanced viscous drag and elastic effects, while the second term represents the contribution of the asymmetric hydrodynamic forces experienced by the spheres over the time intervals $\bar\tau_+$ and $\bar\tau_-$. Equation (39) reduces to Eq. (28) for symmetric morphological adaptations, *i.e.*, in the case $\bar\tau_+ = \bar\tau_-$, $\tilde x_{\mathrm{r},+} = -\tilde x_{\mathrm{r},-}$, and $\langle x_\mathrm{r}^2\rangle_+ = \langle x_\mathrm{r}^2\rangle_-$.

TABLE II. Parameter l_0 that indicates the length at which structural adaptations are activated in simulated motors. Values were obtained from Eq. (41), and are expected to be close to $\langle x_r \rangle$.

Δ	l_0 (R_{min})
0.00	2.3732
0.05	2.4176
0.10	2.4621
0.15	2.5067
0.20	2.5515
0.25	2.5964

We conducted a series of numerical experiments in order to assess the validity of Eq. (39). We used the same numerical integration method described in Sec. 3, where the systematic forces acting the Brownian particles were obtained from $F_i = -\partial\left(\Phi_e + \Phi_c\right)/\partial x_i$. Our new simulations were carried out with parameters $\epsilon = 2k_BT$, $l_{max} = 10R_{min}$, $k = 1\,k_BT/R_{min}^2$, $\eta = 5\sqrt{mk_BT}/R_{min}^2$, and $n = 4$, which makes the interaction between the colloids steep [39]. We simulated motors with the same asymmetry factors used before, $\Delta = 0.00, 0.05, \ldots, 0.25$. With the purpose of giving an approximated value for the parameter l_0, we considered that the elongation of the motor is restricted to small values, $x_r \ll l_{max}$. Thus, we assumed Φ_e to be harmonic. In addition, Φ_c was assumed to represent a hard wall that restricts x_r to be in the region $x_{r.} > \sigma$. This allowed us to calculate l_0 from the canonical distribution, using the approximated potential energies, as

$$l_0 = \frac{\int_\sigma^\infty dx_r\, x_r \exp\left\{-\frac{kx_r^2}{2k_BT}\right\}}{\int_\sigma^\infty dx_r\, \exp\left\{-\frac{kx_r^2}{2k_BT}\right\}} = \sqrt{\frac{2k_BT}{\pi k}}\,\frac{\exp\left\{-\frac{k\sigma^2}{2k_BT}\right\}}{1-\mathrm{erf}\left\{\sqrt{\frac{k\sigma^2}{2k_BT}}\right\}}. \quad (41)$$

The corresponding values for l_0 used in the adaptation algorithm, Eq. (8), were obtained from Eq. (41) and are explicitly shown in Table II.

Firstly, we obtained the time series of $x_r(t)$ for six individual motors simulated over a time interval with size $5 \times 10^5\ u_t$. From these time series we calculated the parameters $\Delta x_{r,\pm}$, $\langle x_r^2 \rangle_\pm$, and $\bar{\tau}_\pm$, appearing in Eq. (39). The resulting values of these quantities are summarized in Table III. On the other hand, α_{eff} was obtained from the examination of the decay of the autocorrelation functions of the variable $x_r(t)$,

$$g(t) = \frac{\langle (x_r(t) - \langle x_r \rangle)(x_r(0) - \langle x_r \rangle)\rangle}{\langle (x_r(0) - \langle x_r \rangle)^2 \rangle},$$

which can be well approximated by a decaying exponential function, whose inverse characteristic time, α_{eff}, was obtained from a nonlinear fitting procedure. Our numerical evidence revealed that α_{eff} does not change systematically with the simulation parameter Δ, *e.g.*, it took the values $0.1384\ u_t^{-1}$ for $\Delta = 0.00$, and $0.1386\ u_t^{-1}$ for $\Delta = 0.25$. Thus, we decided to use the average value of this inverse characteristic time, calculated over the six performed simulations, which turned out to be $\alpha_{eff} = (0.138 \pm 0.008)\, u_t^{-1}$.

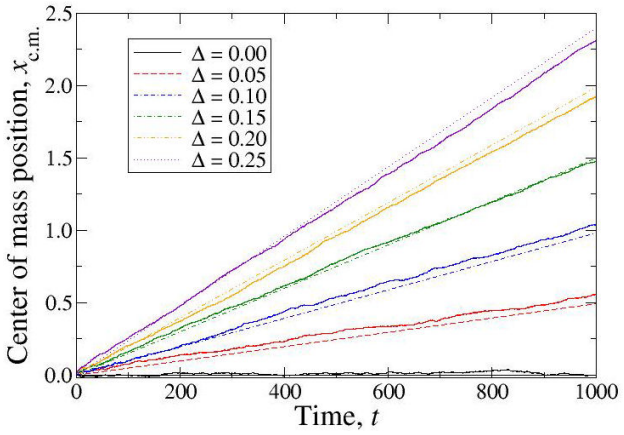

FIGURE 6. Average motion of Brownian motors based on morphological changes and asymmetric molecular potentials. Noisy continuous curves represent the average displacement of an ensemble on 10^3 independent motors. Straight interrupted lines are theoretical estimations obtained from Eq. (39).

In our numerical experiments we verified that the molecular motors based on the use of molecular potentials exhibit directed motion at constant average speeds. This is illustrated in Fig. 6 where we present the resulting average trajectories taken over ensembles of 10^3 molecular motors. In the same Fig. 6, the straight interrupted lines were drawn using the velocities estimated from Eq. (39) and the parameters $\Delta x_{r,\pm}$, $\langle x_r^2 \rangle_\pm$ and $\bar{\tau}_\pm$, presented in Table III, as well as $\alpha_{eff} = 0.138\ u_t^{-1}$. Our estimations of $v_{c.m.}$ are presented in Table IV where they are compared with the values resulting from the simulation experiments, which were obtained from a simple application of the least squares method to the noisy curves in Fig. 6. We found a very good agreement between the calculations based on Eq. (39) and the observed average speed of the simulated motors. It can be noticed from the data in Table IV that velocities derived from Eq. (39) coincide with the experimental velocities, within the uncertainty ranges, for all the used parameters Δ, although deviations between the central values can be recognized, specially at $\Delta = 0.05$ and $\Delta = 0.25$. Nevertheless, such deviations are lower than 6%, and could be considered small. In this case our results would allow us to propose Eq. (39) as a sufficiently good expression for making estimations of the speed of molecular motors operating at asymmetric small morphological changes, $\Delta \leq 0.25$.

TABLE III. Parameters used to estimate $v_{\text{c.m.}}$ from Eq. (39). These quantities were obtained from simulations of individual motors as it is described through the text. Values are reported in simulation units. Statistical uncertainties were found to be $\delta\Delta x_{\text{r},+} = \pm 3 \times 10^{-4}\ R_{\text{min}}$, $\delta\Delta x_{\text{r},-} = \pm 2 \times 10^{-4}\ R_{\text{min}}$, $\delta\langle x_{\text{r}}^2\rangle_+ = \pm 2 \times 10^{-4}\ R_{\text{min}}^2$, and $\delta\langle x_{\text{r}}^2\rangle_- = \pm 1 \times 10^{-4}\ R_{\text{min}}^2$.

Δ	$\Delta x_{\text{r},+}$	$\Delta x_{\text{r},-}$	$\langle x_{\text{r}}^2\rangle_+$	$\langle x_{\text{r}}^2\rangle_-$	$\bar{\tau}_+$	$\bar{\tau}_-$
0.00	0.3035	0.1691	7.1774	4.8097	0.187	0.303
0.05	0.2983	0.1614	7.3542	5.0174	0.187	0.310
0.10	0.2929	0.1567	7.5584	5.2364	0.183	0.303
0.15	0.2990	0.1577	7.8940	5.4766	0.183	0.306
0.20	0.2895	0.1571	8.0919	5.7002	0.177	0.307
0.25	0.2827	0.1498	8.2682	5.9270	0.181	0.303

TABLE IV. Center of mass velocity of molecular motors with different morphological asymmetries. Theoretical estimations were carried out using Eq. (39) and the values of the parameters presented in Table III.

Δ	$v_{\text{c.m.}}$ (simulations, $10^{-4} R_{\text{min}}/u_{\text{t}}$)	$v_{\text{c.m.}}$ (estimated, $10^{-4} R_{\text{min}}/u_{\text{t}}$)
0.00	0	0.00
0.05	5.200 ± 0.003	4.9 ± 0.3
0.10	10.410 ± 0.004	9.8 ± 0.7
0.15	14.690 ± 0.003	15.0 ± 1.0
0.20	19.298 ± 0.004	19.9 ± 1.3
0.25	22.711 ± 0.003	24.0 ± 1.6

5. Competition against a ratchet potential

Finally, we carried out a comparison between the rectifying mechanism based on morphological changes and a classical ratchet potential, in order to show that the former could exhibit larger velocities, even for small values of Δ. We performed the comparison in such a way that our motor will try to overcome the backwards stream of particles created by the ratchet potential. This means that in order to overcome the ratchet's stream, our Brownian motor needs to create a larger net displacement in the opposite direction.

The ratchet potential acting on each of the constituent parts of the molecular motor, $V(x_\mu; t) = \Phi(t)\,\mathcal{V}(x_\mu)$, will be modeled as spatially asymmetric and intermittent. Specifically, it will be defined as in Ref. 46 through

$$\mathcal{V}(x_\mu) = \begin{cases} \frac{h_{\text{rat}}}{a_{\text{rat}}} x_\mu, & \text{if } , 0 < x_\mu < a_{\text{rat}}; \\ \frac{h_{\text{rat}}}{L_{\text{rat}} - a_{\text{rat}}} \left(L_{\text{rat}} - x_\mu\right), & \text{if } a_{\text{rat}} < x_\mu < L_{\text{rat}}; \end{cases} \tag{42}$$

and

$$\Phi(t) = \begin{cases} 0, & \text{if} \quad 0 < t < t_{\text{rat}}; \\ 1, & \text{if} \quad t_{\text{rat}} < t < T_{\text{rat}}. \end{cases} \tag{43}$$

In Eqs. (42) and (43), h_{rat} represents the maximum energy of the ratchet, while L_{rat} and T_{rat} are, respectively, its spatial and temporal periods. The parameter a_{rat} controls the spatial asymmetry of the ratchet, in such a way that for $a_{\text{rat}} < L_{\text{rat}}/2$, it will rectify the Brownian motion to the positive direction, while for $a_{\text{rat}} > L_{\text{rat}}/2$, the mean stream induced by the ratchet will be negative. Finally, the parameter t_{rat} is used to indicate the time interval in which the ratchet remains turned off. This classical operation of the ratchet mechanism is illustrated in Fig. 7.

A first group of simulations was conducted in molecular motors that do not perform morphological changes, this with the purpose of assessing the flow velocity induced by the

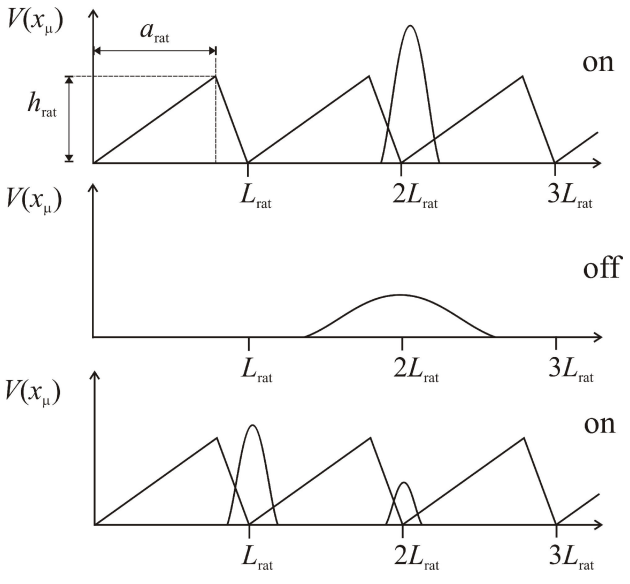

FIGURE 7. The ratchet potential, $V(x_\mu; t)$, used for competition with morphological changes. It has two possible states, on and off, determined by the parameters t_{rat} and T_{rat} in Eq. (43). In the on-state, particles are driven to the minimum energy position, while particle diffuse freely in the off-state. This mechanism together with the spatial asymmetry of V controlled by a_{rat} and L_{rat} in Eq. (42), induce the rectified motion, which for the presented case points to the left. Smooth curves above the x-axis illustrate schematically the PDF for finding the particles at given positions at different times.

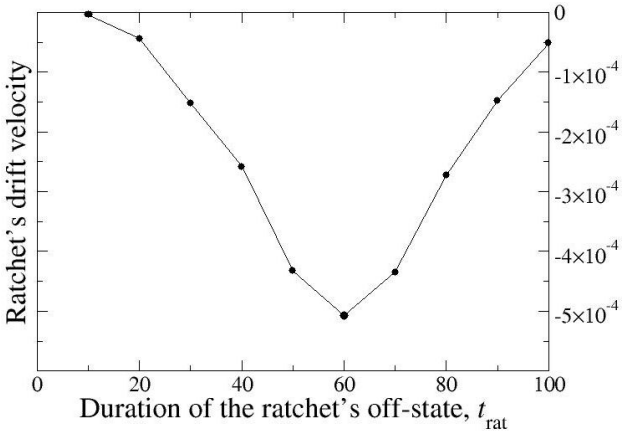

FIGURE 8. Drift velocity induced by the ratchet mechanism with parameters $h_{\text{rat}} = 10k_BT$, $L_{\text{rat}} = 10R_{\text{min}}$, $a_{\text{rat}} = 9R_{\text{min}}$, and $T_{\text{rat}} = 100u_{\text{t}}$, for different values of t_{rat}.

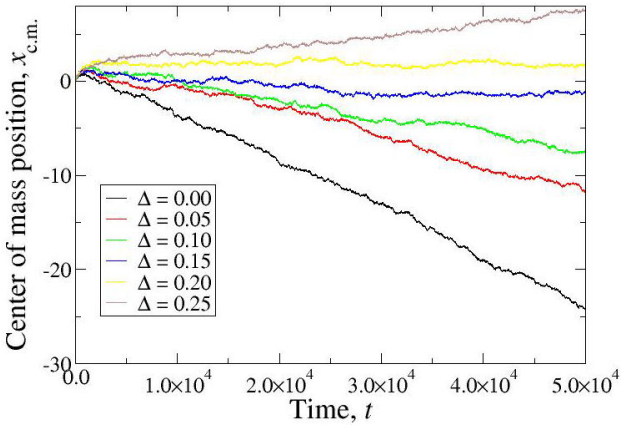

FIGURE 9. Average trajectories of molecular motors under external ratchet forces and antagonistic morphological adaptations characterized by the asymmetry parameter Δ.

ratchet mechanism. In these simulations the ratchet's energy barrier was chosen to be $h_{\text{rat}} = 10k_BT$, which is highly unlikely to be overcome by particles in a thermal bath at temperature T. On the other hand, the spatial parameters were fixed at the values $L_{\text{rat}} = 10R_{\text{min}}$, and $a_{\text{rat}} = 9R_{\text{min}}$. The time period was selected to be $T_{\text{rat}} = 100u_{\text{t}}$, for which we performed ten different experiments varying t_{rat} from 0 to $100u_{\text{t}}$ in regular intervals. The resulting stream velocities were obtained from averages over ensembles of 10^4 inactivated motors. They are shown in Fig. 8 from which it can be observed that the drift velocity is minimized for $t_{\text{rat}} \simeq 60u_{\text{t}}$. Thus, in order to perform a comparison against the motor based on morphological changes, we selected this latter value for all our subsequent experiments. Under such conditions, we activated the morphological changes in molecular motors with repulsive and non-linear interactions, simulated with the same set of parameters described in Sec. 4. As it was the case before, we varied the asymmetry ratio Δ from 0.00 to 0.25 with increments of 0.05. Figure 9 illustrates the mean trajectories obtained from averages of 10^3 motors. It can be noticed that for no morphological adaptations, $\Delta = 0.00$, the center of mass position moves at a constant speed to the left. However, $v_{\text{c.m.}}$ increases as Δ does. Morphological changes finally overcome the ratchet mechanism for $\Delta = 0.25$. The specific velocities obtained in the experiments described above are shown in Table V.

TABLE V. Center of mass velocity of molecular motors with different morphological asymmetries in the presence of a ratchet potential.

Δ	$v_{\text{c.m.}}$ (simulations, $10^{-4}R_{\text{min}}/u_{\text{t}}$)
0.00	-5.074000
0.05	-2.699700
0.10	-1.812000
0.15	-0.471480
0.20	-0.027426
0.25	$+1.119100$

6. Conclusions

We have analyzed the dynamics of a simple intuitive Brownian motor that acquires directed motion from thermal unbiased forces by coordinated morphological modifications. This motor needs to be elastic and to possess adaptable shape. Thermal fluctuations of the surrounding medium promote changes in the elongation of the motor and the information of the length of the system is used by a Maxwell's demon control system to indicate that morphological adaptations must be activated. In turn, the structural modifications of the motor induce unbalanced drag forces that favor the displacement of the motor's center of mass in one direction.

We have used the classical theory of Brownian motion to give an expression for the mean velocity reached by a motor with simple harmonic restitution forces that performs slow morphological adaptations. We expressed this velocity as function of the magnitude of its morphological changes. Our analysis was based on the assumption that these changes are small when compared with the length of the motor itself. This assumption turned out to reduce enormously the mathematical complexity of the problem and allowed us to arrive at closed expressions for the probability distribution functions describing the state of the motor. We verified the applicability of our theoretical treatment using BD simulations. Afterwards, we conducted simulations of more realistic molecular motors conceived as two colloidal particles of controllable size attached by a finite extension chain. We showed by means of BD simulations that they also exhibit directed Brownian motion. In the same manner, we were able to give an expression for the velocity of the molecular motors that works very well for small morphological changes. Finally, we showed that morphological adaptations could produce larger velocities than those obtained from the classical rectifying mechanism based on an external ratchet potential.

It is interesting to perform an estimation of the velocity that could be achieved by an actual motor possessing

the geometrical characteristics used in our model. For this purpose we could consider a molecular motor such that R_{min}=0.1 μm, immersed in a fluid with η=0.01 gcm^{-1}s^{-1}, at $T = 300\,\text{K}$. We can also consider a motor with $l_{\text{max}} = 10\,R_{\text{min}}$, restitution coefficient selected according to the so-called extensibility parameter [41], $b = kl_{\text{max}^2}/k_BT = 50$. By assuming that $(1-2\zeta\bar{\tau})\,\Delta/6\sqrt{2}\pi^{3/2} \sim 10^{-4}$, we obtain, from Eq. (28), that $v_{\text{c.m.}} \sim 10^{-2}\mu\text{m s}^{-1}$.

We do not know whether natural or artificial microscopic systems exist that presents directed Brownian motor behavior based on the mechanisms proposed in the present paper. We stress that biological systems that propel themselves in fluid environments by performing morphological changes resembling those described in Fig. 1, such as certain protozoa and species of Euglena (see the discussion in Ref. 31 for further details), can not be considered as physical realizations of our model, since in such systems contractions and expansions are not driven by thermal fluctuations but by an internal mechanism that can be theoretically treated as a piston [31]. However, it is worth noticing that some microscopic systems exist that possess the characteristics needed by the components of our theoretical motor. In particular, differences in viscous drag between different parts of a larger microstructure could be obtained from conformational or configurational changes that are induced in artificial molecular machines by diverse stimuli, *e.g.*, light, electrochemistry, heat, allosteric effects, or temperature [42]. Some specific molecular structures with conformational changes have been presented as potential solutions to proposed designs for theoretical nanoswimmers [42, 43]. On the other hand, the activation of these configurational changes could be controlled using a Maxwell's demon, similar to those that raise and lower an energy barrier by using the information of the location of a macrocycle over a long rod-shaped molecule [44]. Experimental implementations of such mechanism have been conducted using photo and chemically activated barriers [45, 46].

In this paper, some issues that could be relevant for understanding the dynamics of the proposed Brownian motor have not been considered. They include a detailed non-equilibrium Thermodynamics analysis of its operation and efficiency, and an analysis of the effects induced by the hydrodynamic memory of its environment, similar to those calculated for single Brownian particles [47]. Such effects will be taken into account in subsequent publications.

Acknowledgements

H. Híjar thanks La Salle University Mexico for financial support under grant NEC-04/15.

1. S. Chandrasekhar, *Rev. Mod. Phys.* **15** (1943) 1.
2. R.P. Feynman, R.B. Leighton and M. Sands, *The Feynman Lectures on Physics* (Addison Wesley, Reading, MA, 1966) **Vol. 1** chapt. 46.
3. M.O. Magnasco, *Phys. Rev. Lett.* **71** (1993) 1477.
4. M. Von Smoluchowski, *Phys. Z.* **XIII** (1902) 1069.
5. P. Hänggi and R. Bartussek, *Brownian rectifiers: how to convert Brownian motion into directed transport*, in *Nonlinear Physics of Complex Systems* (Berlin: Springer 1996) p. 294.
6. P. Hänggi, F. Marchesoni, and F. Nori, *Ann. Phys. (Leipzig)* **14** (2005) 51.
7. P. Hänggi and F. Marchesoni *Rev. Mod. Phys.* **81** (2009) 387.
8. P. Nelson, *Biological Physics. Energy, Information, Life* W.H. Freeman and Company, (New York 2014).
9. K. Svoboda, C.F. Schmidt, B.J. Schnapp and S.M. Block, *Nature* **365** (1993) 721.
10. H. Lodish *et al*., *Molecular Cell Biology*, 4th edition, (W. H. Freeman, New York, 2000).
11. H. Noji, R. Yasuda, M. Yoshida and K. Kinosita Jr., *Nature* **386** (1997) 299.
12. D. Sabbert, S. Engelbrecht and W. Junge, *Proc. Natl. Acad. Sci. U. S. A.* **94** (1998) 4401.
13. P.D. Boyer, *Annu. Rev. Biochem.* **66** (1997) 717.
14. S.S. Patel and I. Donmez, *Journal of Biological Chemistry* **281** (2006) 18265.
15. D.S. Johnson, L. Bai, B.Y. Smith, S.S. Patel and M.D. Wang, *Cell* **129** (2007) 1299.
16. P.M. Hoffmann, *Life's Ratchet* (Basic Books, 2012, New York).
17. P. Reimann and P. Hänggi, *App. Phys. A* **75** (2002) 169.
18. P. Reimann, *Phys. Rep.* **361** (2002) 57.
19. G.G. Stokes, *Trans. Camb. Philos. Soc.* **8** (1847) 441.
20. H. Risken, *The Fokker-Planck Equation* (Springer, Berlin, 1984).
21. S.J. Ebbens and J.R. Howse, *Soft Matter* **6** (2010) 726.
22. D. Patra, S. Sengupta, W. Duan, H. Zhang, R. Pavlick and A. Sen *Nanoscale* **5** (2013) 1273.
23. J. Rousselet, L. Salome, A. Ajdari and J. Prost, *Nature* **370** (1994) 446.
24. C. Kettner, P. Reimann, P. Hänggi and F. Müller, *Phys. Rev. E* **61** (2000) 312.
25. S. Matthias and F. Müller, *Nature* **424** (2003) 53.
26. S. Sundararajan, P.E. Lammert, A.W. Zudans, V.H. Crespi and A. Sen, *Nano Lett.* **8** (2008) 1271.
27. L. Baraban *et al*., *Nano* **6** (2012) 3383.
28. S. Martel, *Magnetoactic Bacteria for Microrobotics*, in *Microrobotics. Biologically Inspired Microscale Robotic Systems*, M. Kim, A.A. Julius and E. Steager, editors, (Elsevier, Oxford, 2012).
29. A. Najafi and R. Golestanian, *Phys. Rev. E* **69** (2004) 062901.

30. J.E. Avron, O. Kenneth and D.H. Oaknin, *Phys. Rev. E* **69** (2004) 232.

31. J.E. Avron, O. Gat and O. Kenneth, *Phys. Rev. Lett.* **93** (2004) 186001.

32. F. Ambía and H. Híjar, *JPCS* **738** (2016) 012037.

33. G.K. Batchelor, *An introduction to fluid dynamics*, (Cambridge University Press, New York, 2000).

34. H. Híjar, *J. Chem. Phys.* **139** (2013) 234903.

35. D.S. Grebenkov, *J. Phys. A* **48** (2014) 013001.

36. J.K.G. Dhont, *An introduction to dynamics of Colloids*, (Elsevier, Amsterdam, 2003).

37. M.E.J. Newman, *Contemporary Physics* **46** (2005) 323.

38. D. Weeks, D. Chandler and H.C. Andersen, *J. Chem. Phys.* **54** (1971) 5237.

39. J.T. Padding and A.A. Louis, *Phys. Rev. E* **74** (2006) 041402.

40. J. Prost and J.F. Chauwin, *Phys. Rev. Lett.* (1994).

41. A.P.G. van Heel, M.A. Hulsen and B.H. A.A. van den Brule, *J. Non-Newtonian Fluid Mech.* **75** (1998) 253.

42. S. Erbas-Cakmak, D.A. Leigh, C.T. McTernan, and A.L. Nussbaumer, *Chem. Rev.* **115** (2015) 10081.

43. E.R. Kay, D.A. Leigh, and F. Zerbetto, *Angew. Chem. Int. Ed.* **46**(2007) 72.

44. R.D. Astumian, *Annu. Rev. Biophys.* **40** (2011) 289.

45. M. Alvarez-Perez, S.M. Goldup, D.A. Leigh, and A.M.Z. Slawin, *J. Am. Chem. Soc.* **130** (2008) 1836.

46. V. Serreli, C.F. Lee, E.R. Kay, and D. A. Leigh, *Nature* **445** (2007) 523.

47. H. Híjar, *Phys. Rev. E* **91** (2015) 022139.